

Coarse-Grained Molecular Dynamics Simulations for Oxidative Aging of Polymers under Various O₂ Concentrations

*Takato Ishida**, Kazuya Haremakei, Yusuke Koide, Takashi Uneyama, Yuichi Masubuchi

Department of Materials Physics, Nagoya University, Furo-cho, Chikusa, Nagoya 464-8603, Japan

* E-mail: ishida@mp.pse.nagoya-u.ac.jp

ABSTRACT

Modeling of polymer oxidative aging has been actively studied since the 1990s. Insights from these studies suggest that the transport of oxygen and radicals significantly influences aging heterogeneity, alongside chemical reaction kinetics. A recent simulation study [Ishida et al., *Macromolecules*, 56(21), 8474-8483, 2023] demonstrated that mesoscale heterogeneity arises when the H-abstraction reaction occurs faster than the relaxation times of polymer chains. In this study, the simulations were extended by modeling the rate of oxygen addition to polymer radicals (k_2) to reflect the effects of the O₂ concentration. Three key aspects of oxidative aging behavior were found to be influenced by the O₂ addition rate: (i) reaction kinetics, (ii) the degree of heterogeneity, and (iii) amount of crosslinking. Namely, reducing O₂ concentration slows the conversion of polymer radicals into H-abtractable peroxy radicals. This deceleration delays H-abstraction reactions, increases the number of polymer radicals, and promotes crosslinking reactions between two polymer radicals.

KEY WORDS

Degradation / Coarse-grained simulations / Polymer dynamics / Auto-oxidation / Radical dynamics

1. INTRODUCTION

There is no doubt that O_2 concentration plays a crucial role in polymer oxidative aging, as confirmed by several experimental works [1–4]. The significance of O_2 originates from the fact that the reaction mechanism governing oxidative aging is represented by the "closed-loop mechanistic scheme" (CLMS) [5–10] based on autoxidation reactions [11,12]. Numerous studies have successfully described the kinetics of oxidative aging reactions through kinetic modeling based on the CLMS [5–10]. This framework has significantly advanced the modeling of aging processes at the microscopic reaction level. The reaction rate of O_2 addition to a polymer radical ($P\cdot$), a key parameter in the CLMS, is proportional to O_2 concentration, reflecting the reaction rate constant for O_2 addition (so-called k_2) [11].

Another critical aspect is the diffusion-limited oxidation (DLO) effect [13], which induces macroscopic heterogeneity in aging behavior along the thickness direction of the sample. DLO arises when oxygen consumption exceeds the O_2 supply, lowering the internal O_2 concentration relative to the surrounding environment. DLO systems can be numerically analyzed using a continuum field framework that accounts for material transport and reaction kinetics, with previous studies reporting simulations based on the finite element method (FEM) [10,13]. In such approaches, the dynamics of polymers are not explicitly considered. However, aging reactions are intrinsically linked to the transport of macroradicals governed by polymer chain dynamics [14]. Thus, DLO simulations should incorporate a heterogeneous O_2 concentration field into a model capable of considering polymer dynamics, performed on a system size large enough to observe DLO effects (typically at the sub-mm scale [10]). There are two approaches to appropriately handle the above considerations. One is to simulate a system with a very large size and explicitly solve the O_2 molecule dynamics or the O_2 concentration field. The other is to employ a relatively small system size, assuming the O_2 concentration as a homogeneous field, and combining it with a conventional continuum field framework for scaling up. The former approach is impractical as it requires computational resources on an unfeasibly large scale. In contrast, the latter approach allows the effects of O_2 concentration to

be represented by modifying the reaction rate of the O₂ addition reaction in the CLMS, making simulations feasible with realistic computational resources. Therefore, it is valuable to deepen our insights into oxidative aging simulations in mesoscale systems with varying O₂ concentrations.

Recently, we developed a coarse-grained molecular dynamics simulation (CGMD) capable of appropriately handling oxidative aging, including polymer segment and radical dynamics. In our previous studies [14,15], for simplicity, we performed simulations under oxygen excess conditions, known as the OER (Oxygen Excess Regime). As mentioned above, it is crucial to develop an aging simulation framework capable of accommodating changes in O₂ concentration. This study updates the aging simulation by examining the effects of O₂ concentration through variations in the O₂ addition rate to polymer radicals, focusing on its impact on reaction kinetics and aging heterogeneity.

2. MODELS AND SIMULATIONS

In this study, molecular dynamics calculations follow a framework of previous works [14,15]. To incorporate O₂ concentration dependence, only the set of chemical reactions (oxidation) and reaction kinetic parameters are modified from those in prior works [14,15]. In this model, polymer chains are represented using the Kremer-Grest (KG) model [16], with the total potential determined by the sum of the finite extensible nonlinear elastic (FENE) spring potential (U_{FENE}) between chemically bonded beads, and the Weeks-Chandler-Andersen potential (U_{WCA}) acting between all particles. U_{FENE} and U_{WCA} are expressed as follows.

$$U_{\text{FENE}}(r) = \begin{cases} -0.5kR_0^2 \ln \left[1 - \left(\frac{r}{R_0} \right) \right], & r \leq R_0 \\ \infty, & r > R_0 \end{cases} \quad (1)$$

$$U_{\text{WCA}}(r) = \begin{cases} 4\varepsilon \left[\left(\frac{\sigma}{r} \right)^{12} - \left(\frac{\sigma}{r} \right)^6 + \frac{1}{4} \right], & r \leq 2^{1/6}\sigma \\ 0, & r > 2^{1/6}\sigma \end{cases} \quad (2)$$

In these equations, r is the distance between interacting or chemically bonded beads, ε is the

WCA energy parameter, and σ represents the bead diameter. k is the FENE spring constant and R_0 corresponds to the maximum bond length. These parameters are chosen as the same as the standard settings of the KG model [16], being $R_0 = 1.5\sigma$, $k = 30\varepsilon/\sigma$, and $\rho^* = 0.85/\sigma^3$. The position of each bead obeys the Langevin equation, which describes the balance among inertia, conservative, drag, and random forces, as written below.

$$m \frac{d^2 \mathbf{r}_i}{dt^2} = - \frac{\partial U_{\text{tot}}}{\partial \mathbf{r}_i} - \Gamma \frac{d\mathbf{r}_i}{dt} + \mathbf{W}_i(t) \quad (3)$$

where m is the mass of the bead, and \mathbf{r}_i is the position of the i -th bead. Γ is the bead friction coefficient, set to 1.0 in this study. $\mathbf{W}_i(t)$ represents Gaussian random force that satisfies $\langle \mathbf{W}_i(t) \rangle = 0$ and $\langle \mathbf{W}_i(t) \mathbf{W}_j(t') \rangle = 2k_B T \Gamma \delta_{ij} \delta(t - t') \mathbf{I}$. k_B is the Boltzmann constant and T is the temperature. Here, $\langle \dots \rangle$ indicates the statistical average and \mathbf{I} is the unit tensor. U_{tot} is the total potential of the system written as:

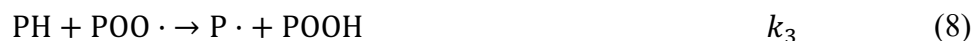
$$U_{\text{tot}} = \sum_{i>j} U_{\text{WCA}}(r_{ij}) + \sum_{i,j \in S_{\text{bond}}} U_{\text{FENE}}(r_{ij}) \quad (4)$$

where r_{ij} is defined as $r_{ij} = |\mathbf{r}_i - \mathbf{r}_j|$, and S_{bond} represents the set of bonded pairs of beads.

In this work, the bead mass is set to $m = 1$, with the units of length, energy, and time defined as σ , ε , and $\tau = \sigma \sqrt{m/\varepsilon}$, respectively. The temperature is set to $k_B T = 1$. Here, a cubic simulation box with a side length 67.2 is considered under periodic boundary conditions. A polymer melt system consisting of 2560 Kremer-Grest chains with a polymerization degree of $N = 100$ is placed in the simulation box. Numerical integration of the Langevin equation is performed with a time step of $\Delta t = 0.005$, and all simulations in this study are conducted in the NVT ensemble.

The oxidation reactions in this simulation are based on a CLMS-derived set of chemical reactions [2,6,17]. Except for the inclusion of an additional O_2 addition reaction to polymer radicals, the

reaction mechanisms considered are consistent with previously reported chemical reactions for the thermal oxidative aging of polypropylene (PP) [14,15].



Here, $\text{P} \cdot$ denotes a polymer radical, $\text{PO} \cdot$ represents an alkoxy radical, and $\text{POO} \cdot$ is a peroxy radical, all of which are types of macroradicals attached to polymer chains (Figure 1). POOH corresponds to a hydroperoxide group on polymer chains, while $\cdot \text{OH}$ represents a free radical.

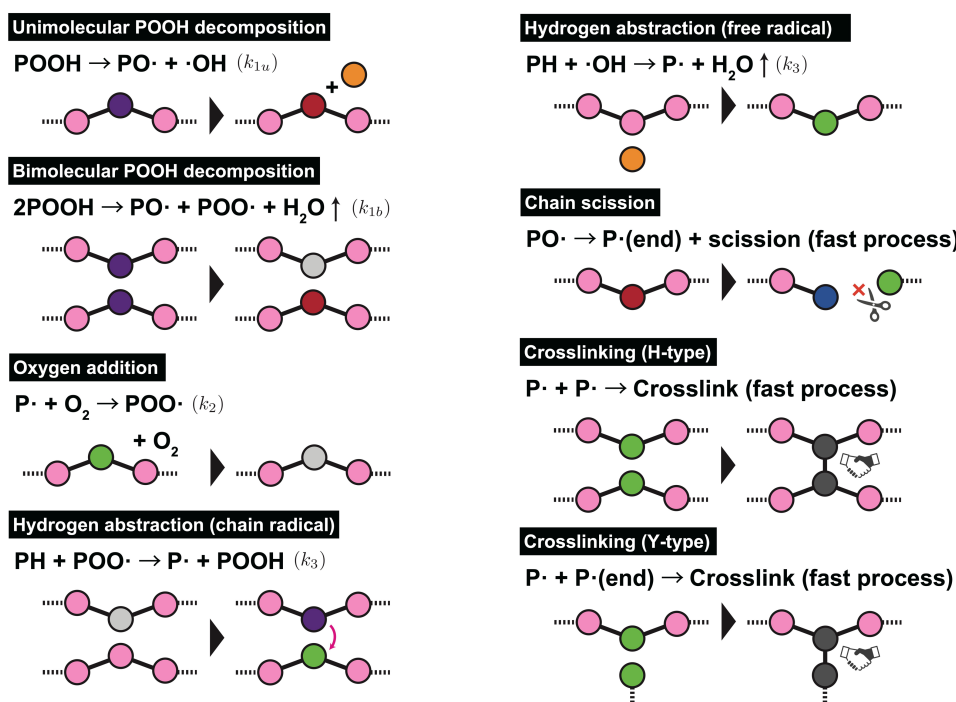


Figure 1 Schematic representation of oxidation reaction topology. PH (polymer substrate): pink, POOH (hydroperoxide): purple, PO· (alkoxy radical): red, ·OH (free radical): orange, P· (polymer radical): green, POO· (peroxy radical): white, scission end: blue, crosslinked beads: gray.

Among the chemical reactions considered, the low-molecular-weight species excluding polymer segments are O₂, OH·, and H₂O. In this work, the dynamics of O₂ molecules are not explicitly solved. Consequently, the O₂ concentration, as a control parameter in this study, is introduced as a uniform O₂ concentration field in the system. Thus, O₂ addition reactions can be treated as first-order kinetics scaled by O₂ concentration. On the other hand, ·OH beads are modeled as being driven by the Langevin equation without interacting with other particles. Although the diffusivity of ·OH only depends on the friction it experiences from the surrounding medium, it is known that this friction coefficient has a limited impact on oxidative aging [15]. Thus, we assign ·OH beads a sufficiently low friction coefficient, enabling them to traverse distances beyond the system size within the average time ($\sim 1/k_3$) before deactivating through H-abstraction reaction. H₂O molecules generated during oxidation are immediately removed from the system and are not included in the dynamics calculations.

Here, chemical reactions are modeled to occur stochastically when the reaction topology shown in Figure 1 is satisfied. The reaction cutoff distance is set to $r_{\text{cutoff}} = 2^{1/6}$. The rates of considered reactions (k_{1u}, k_{1b}, k_2, k_3) are presented along with their corresponding reaction equations, assuming that the reaction topology is satisfied. For reactions labeled as “fast process” in Figure 1, where $k_{(\cdot)}$ values are not specified, the reaction occurs immediately upon satisfying the reaction topology. The reaction kinetics are mapped onto the timescale of this simulation using parameters from previously reported thermal-oxidative aging of PP at 180 °C [2,6,17]. To investigate the effects of O₂ concentration on aging heterogeneity, the same parameter set as in prior studies [14,15] (with the exception of k_2)—where H-abstraction occurs before chain relaxation—was employed. If the reaction topology shown in Figure 1 is satisfied, the reaction rates expressed in the simulation time unit τ are as follows: $k_{1u} = 1.6 \times 10^{-5}/\tau$, $k_{1b} = 5.8 \times 10^{-4}/\tau$, $k_3 = 1.0 \times 10^{-1}/\tau$, and the

initial (unaged) KG chain relaxation time $\tau_{R_0} = 2 \times 10^4 \tau$.

We perform aging simulations under various O_2 concentration conditions. Since the O_2 concentration in the system is proportional to the rate of the O_2 addition reaction k_2 [2], oxidative aging simulations are conducted for several O_2 concentrations by systematically varying k_2 . Here, four cases of $k_2 \tau$ are considered: 5.0×10^{-4} , 2.5×10^{-3} , 2.5×10^{-2} and 5.0×10^{-2} . The maximum k_2 case is set to align with the kinetic model for the onset of OER in previous studies [2,6,17]. In OER case of $k_2 \tau = 5.0 \times 10^{-2}$, the generated $P\cdot$ immediately undergoes O_2 addition and is converted to $POO\cdot$. In non-OER cases, the probability of this reaction is adjusted based on k_2 to introduce a delay in the conversion of $P\cdot$ to $POO\cdot$.

In this study, simulations were performed using Large-scale Atomic/Molecular Massively Parallel Simulation (LAMMPS), version 23Jun22 [18], with chemical reactions incorporated into the dynamics calculations via the REACTION package [19,20]. As in the previous works [14,15], the system was initialized from a fully relaxed state using a combination of the fast push-off and double-bridging methods. Initially, all beads were PH, but one bead was substituted with POOH, and the oxidative aging simulation started at $t = 0$ when this POOH bead decomposed.

3. RESULTS AND DISCUSSION

Figure 2 shows snapshots of oxidative aging simulations at different k_2 , projected onto the xy -plane. Here, the conversion ratio α is defined as the residual fraction of PH beads, specifically $\alpha = 1 - \frac{N_{PH}(t)}{N_{PH_0}}$, where $N_{PH}(t)$ is the number of PH beads at time t , and N_{PH_0} is the initial number. In Figure 2, only scission ends, $P\cdot$, and $POO\cdot$ beads are visualized, and the bead size is displayed larger than the actual size (1σ) for clarity. The areas appearing as blank domains are actually filled with other types of beads, such as PH or POOH. The snapshots reveal that when $k_2 \tau = 5.0 \times 10^{-2}$, the distribution of scission sites is highly heterogeneous. This phenomenon occurs because, as discussed in previous studies [14,15] under OER conditions, H-abstraction reaction by $POO\cdot$ radicals precedes chain relaxation. Conversely, as k_2 decreases, the number of $P\cdot$ radicals increases, and the spatial

distribution of aged domains becomes more uniform. The average time for $P\cdot$ to convert to $POO\cdot$ (H-abtractable) via O_2 addition process is $1/k_2$. When k_2 is low, radicals remain in the $P\cdot$ state and tend to diffuse over longer distances. Even if the H-abstraction rate becomes larger than the average chain relaxation rate, the aging heterogeneity is somewhat mitigated due to decreased O_2 concentration. This characteristic aspect reflects the essential nature of O_2 concentration dependence in heterogeneous oxidative aging.

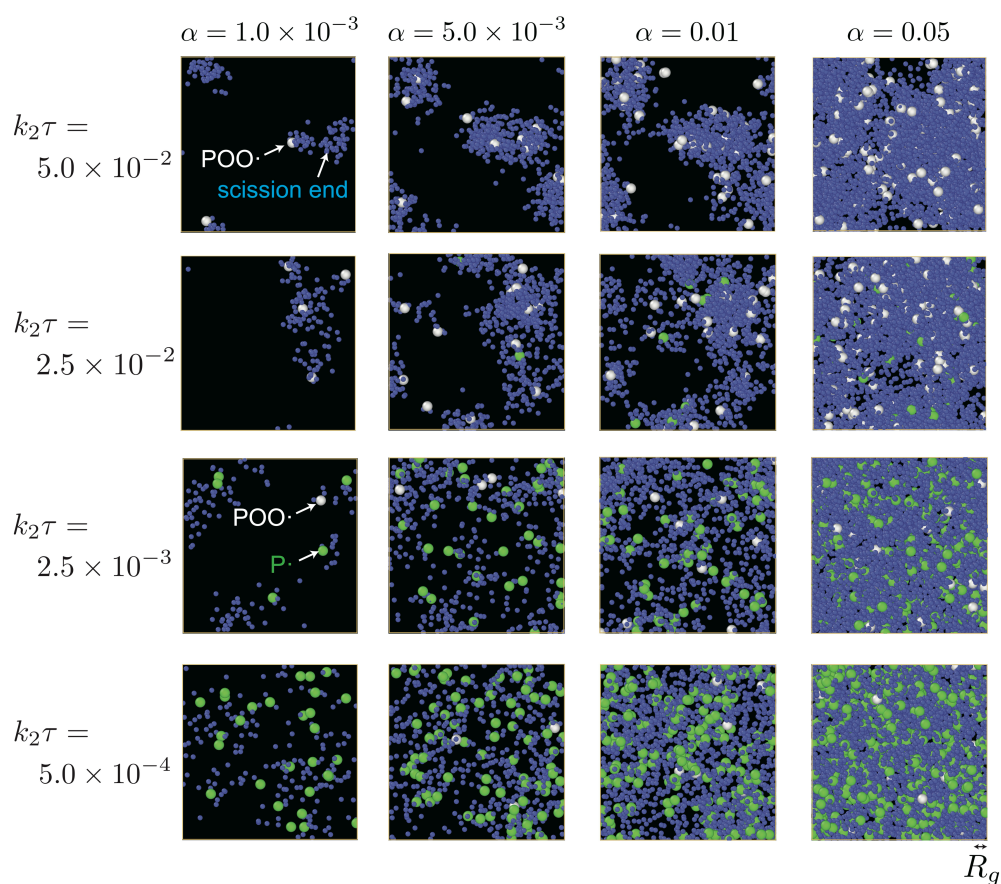


Figure 2 Snapshots from the oxidation aging simulations at various conversion levels $\alpha \left(= 1 - \frac{N_{PH}(t)}{N_{PH0}} \right) = 1.0 \times 10^{-3}, 5.0 \times 10^{-3}, 0.01, 0.05$ under different k_2 conditions. Green beads represent $P\cdot$ (polymer radicals), white beads indicate $POO\cdot$ (peroxy radicals), and blue beads show scission sites. Black areas are filled with unreacted polymers.

Figure 3 presents the chemical reaction kinetics. Each plot exhibits autocatalytic behavior involved

with an induction period, where the reaction accelerates as the concentration of the unstable product POOH (radical source) and the total amount of radicals increase. The kinetics exhibit a clear dependence on O₂ concentration, with lower k_2 leading to retardation of the oxidative aging kinetics. The O₂ concentration dependence of chemical kinetics is qualitatively consistent with experimental findings reported [1,2,21]. It is well known that the kinetics of oxidative aging kinetics are predominantly governed by the rate of H-abstraction reaction by POO· radicals [11]. In this study, we confirm that changes in k_2 alter the O₂ addition rate of P· → POO·, resulting in an increased ratio of P· to POO· at lower O₂ concentration conditions, as shown in Figure 4(a). Additionally, the rate of crosslinking reactions depends on the amount of P·. Although POO· may contribute to unstable crosslinks, such as POOP or P(OO)OP, their high instability renders them negligible in the examined conditions [11,22]. Consequently, with lower k_2 values, where P· is more prevalent, the ratio of crosslinking to chain scission ($N_{\text{crosslink}}/N_{\text{end}}$) increases, as shown in Figure 4(b). In contrast, almost no crosslinking occurred under OER conditions. In case of high-temperature thermo-oxidative aging, particularly near the sample surface where O₂ consumption is intense, the DLO effect often causes a decrease in the O₂ concentration within the bulk region of polymeric materials [13,23]. This effect is frequently discussed in macro-scale oxidative aging experiments [1,13,23–26]. Among these studies, experiments have reported that regions exhibiting the DLO effect tend to show a higher rate of crosslinking and a shift in the scission-to-crosslinking ratio toward crosslink dominance [24–26]. Our study successfully replicates these experimental observations.

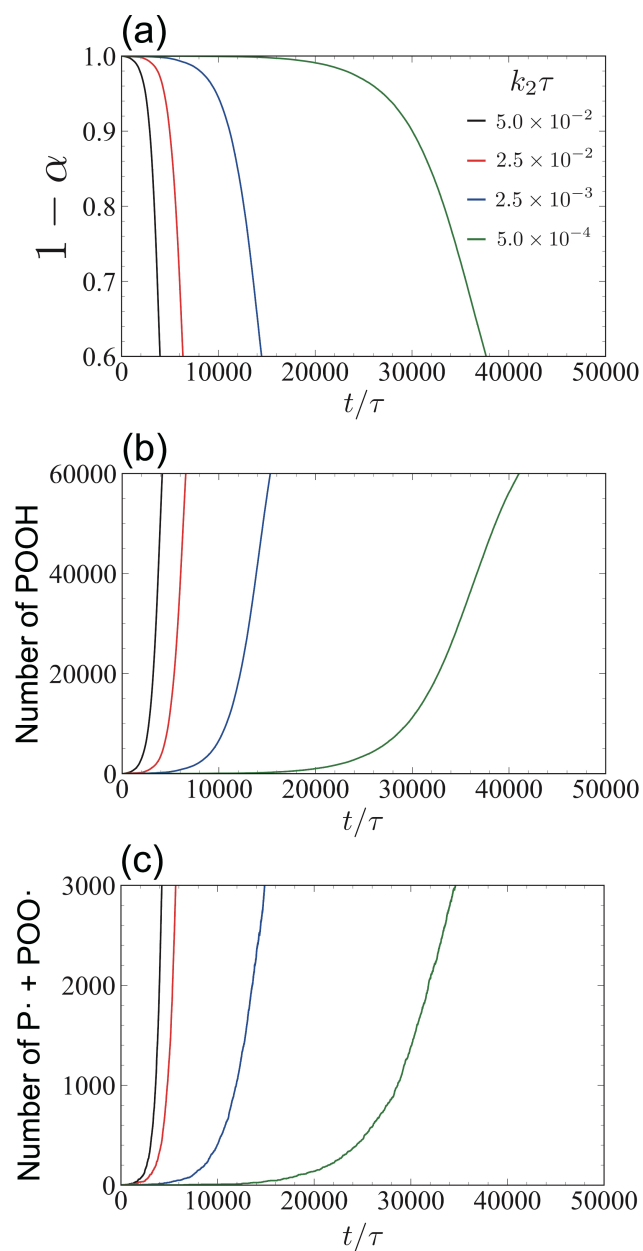


Figure 3 Time evolution of (a) the conversion $1 - \alpha = \frac{N_{\text{PH}}(t)}{N_{\text{PH}_0}}$, (b) the number of POOH beads, and (c) the number of radical beads ($P\cdot + POO\cdot$).

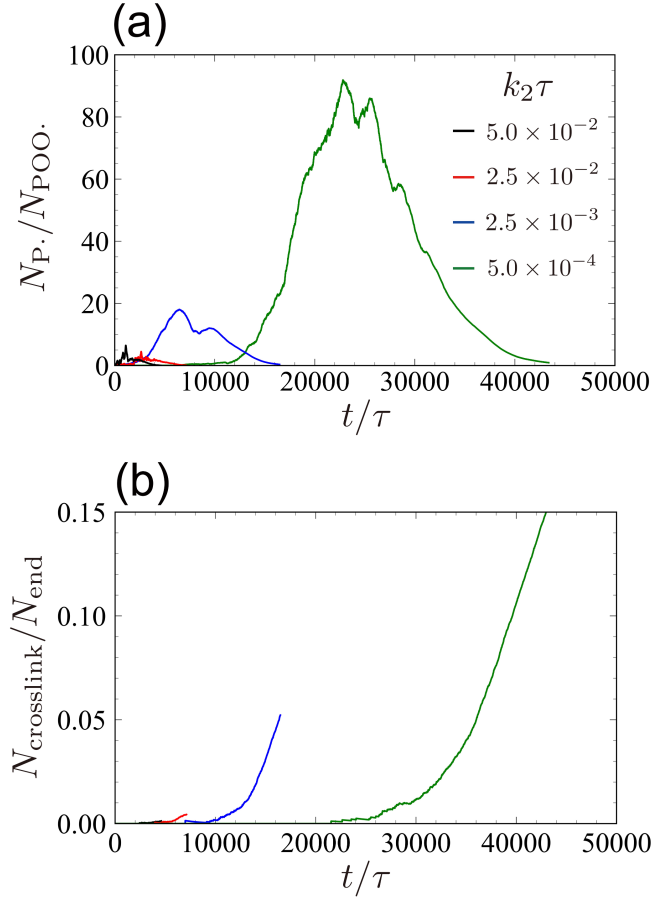


Figure 4 Time evolution of (a) the ratio of P· to POO· radicals ($N_{P\cdot}/N_{POO\cdot}$), and (b) the ratio of crosslink to scission end counts ($N_{\text{crosslink}}/N_{\text{end}}$) under various k_2 conditions.

Figure 5 illustrates the dependence of the induction period (t_{ind}) and reaction time (t_{react}) on O_2 addition rate. The induction period is defined according to our previous work [15], and the reaction time is defined as the duration from t_{ind} to reaching $\alpha = 0.5$. Both t_{ind} and t_{react} increase as k_2 decreases. They exhibit power-law behavior with respect to O_2 concentration, following the relations $t_{\text{ind}} \propto k_2^{-0.45}$ and $t_{\text{react}} \propto k_2^{-0.42}$, respectively. The impact of the O_2 concentration for the induction period in thermo-oxidative aging of PP has been experimentally demonstrated by Heude et al. [21]. Our simulations qualitatively capture this behavior. The aging kinetics of oxidative aging proceed through an accelerated period, and experimental evaluation of t_{react} for high α is challenging due to the volatilization of oxidized products and its uncertainty in molar extinction coefficients (in the case of infrared spectroscopy) [27]. Nevertheless, simulations provide a clear

depiction of k_2 dependence of t_{react} . The retardation of aging kinetics described above arises from differences in the H-abstraction reaction rate. The rate of this reaction is influenced by the number of $\text{POO}\cdot$ radicals and the spatial coordination of PH beads around $\text{POO}\cdot$ radicals. The latter contribution can be evaluated through the radial distribution function ($g_{\text{PH-POO}}(r)$) between PH and $\text{POO}\cdot$. Figure 6 presents $g_{\text{PH-POO}}(r)$ at a conversion level of $\alpha = 0.1$ under different k_2 conditions. According to the results, there is no noticeable k_2 dependence in the local arrangement of PH around $\text{POO}\cdot$. This indicates that the kinetics of oxidative aging are predominantly governed by the number of $\text{POO}\cdot$ radicals present in the system. In low k_2 cases, the reduced number of $\text{POO}\cdot$ radicals leads to a retardation of the overall chemical kinetics. Additionally, the power-law exponents of t_{ind} and t_{react} with respect to k_2 are both weaker than -1, indicating that the reaction kinetics are not dominated by a single reaction. One possible factor is that as k_2 decreases, the concentration of $\text{P}\cdot$, the reactant in O_2 addition reaction, increases. Therefore, the overall reaction kinetics cannot be reduced to a single curve using $k_2 t$ (Figure S1 in Supporting Information). However, by normalizing with t_{ind} , the results from simulations with different k_2 values are shown to align on a comparable timescale (Figure S2). Nonetheless, the clear k_2 -dependence of the ratio of $\text{P}\cdot$ to $\text{POO}\cdot$ radicals and the ratio of crosslink to scission end counts is preserved (Figure S3, S4).

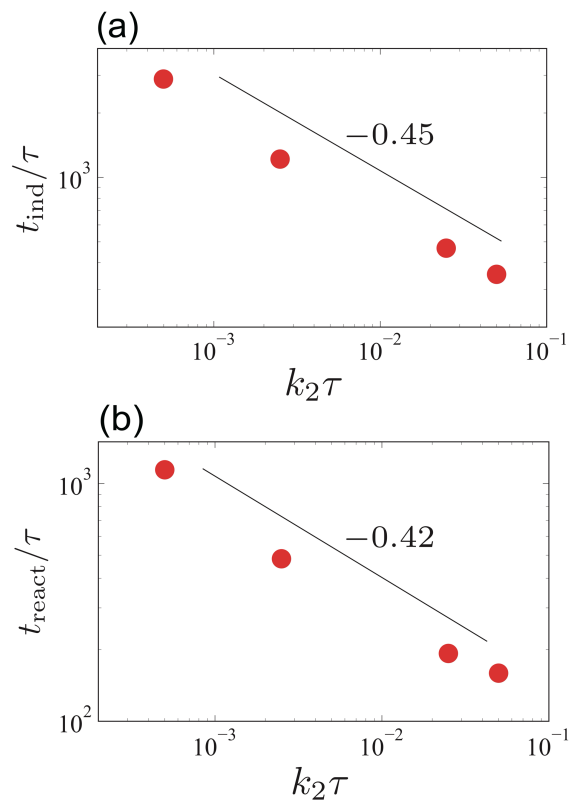


Figure 5 O₂ addition rate k_2 dependence of (a) t_{ind} and (b) t_{react} . The figure displays the average results from 16 simulations initiated from different initial configurations and random seeds.

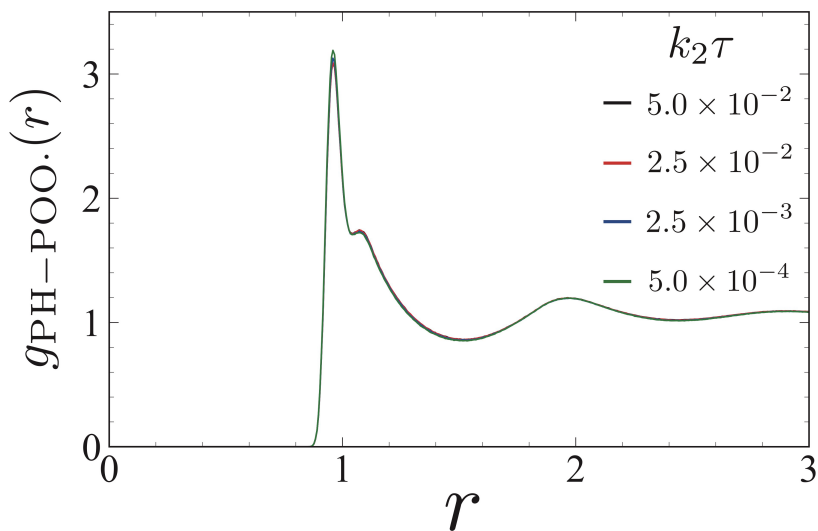


Figure 6 Radial distribution functions ($g_{\text{PH-POO}}(r)$) between PH and POO \cdot at $\alpha = 0.1$.

Next, we focus on the effect of the O₂ addition rate on the spatial heterogeneity of oxidative aging.

Figure 7 presents the static structure factor $S(q)$ calculated between scission sites. An upturn

observed in the low- q region of $S(q)$ indicates spatial heterogeneity [28]. A clear dependence of heterogeneity on k_2 was identified, consistent across both low and high α regions. As aging progresses, the heterogeneity diminishes. This phenomenon, as previously reported [14,15], is attributed to the accelerated relaxation and enhanced molecular chain mobility due to oxidative chain scissions. In low- k_2 cases, the retardation of H-abstraction reactions causes radical diffusion to predominate over localized reaction progression, thereby explaining the observed reduction in heterogeneity with decreasing of O_2 concentrations.

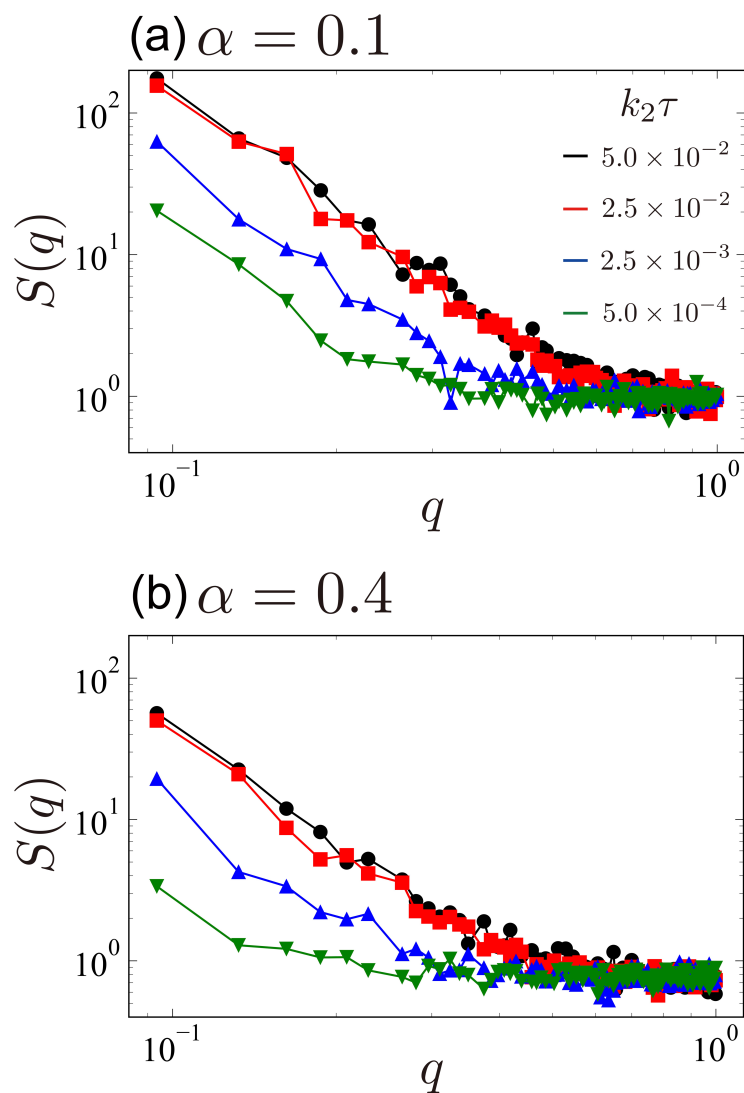


Figure 7 Static structure factor $S(q)$ between scission end beads for various k_2 cases: (a) $\alpha = 0.1$ (low conversion region), (b) $\alpha = 0.4$ (high conversion region).

Let us next consider another aspect reflecting the heterogeneity of oxidative aging: the spatial fluctuations of local conversion. As in our previous study [15], the spatial fluctuation of the local conversion is expressed using the number of remaining PH beads as follows.

$$\delta = \frac{\sqrt{\langle (N_{\text{PH}}^{(i)})^2 \rangle - \langle N_{\text{PH}}^{(i)} \rangle^2}}{\langle N_{\text{PH}}^{(i)} \rangle} \quad (13)$$

Here, we envisage the target simulation box divided into 20 subcells along each edge, resulting in 8000 small cubic regions. We focus on the fluctuations in the number of PH beads, $N_{\text{PH}}^{(i)}$, present in the i -th domain. This fluctuation δ is equivalent to the fluctuation in the local conversion α_{local} . Figure 8 presents the spatial fluctuations of the local conversion, δ , for different k_2 cases. The fluctuation δ , reflecting aging heterogeneity, increases with higher k_2 conditions. This trend is consistent with the behavior observed in $S(q)$ calculated between scission sites.

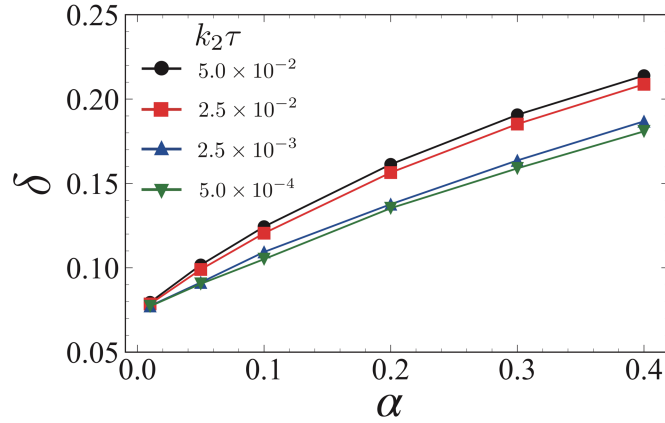


Figure 8 Spatial fluctuation δ for the number of PH beads, corresponding to the fluctuation of local conversion in oxidative aging.

The effect of k_2 extends to the chain length distribution, as shown in Figure 9. This figure illustrates the chain length distribution at $\alpha = 0.1$. When comparing the distributions at the same

conversion level, it was observed that as k_2 decreases, the distribution broadens in the range of chain lengths between 5 and 30. This behavior is likely attributed to the enhanced impact of crosslinking between $P\cdot$ radicals under lower O_2 concentration conditions (see Figure 4).

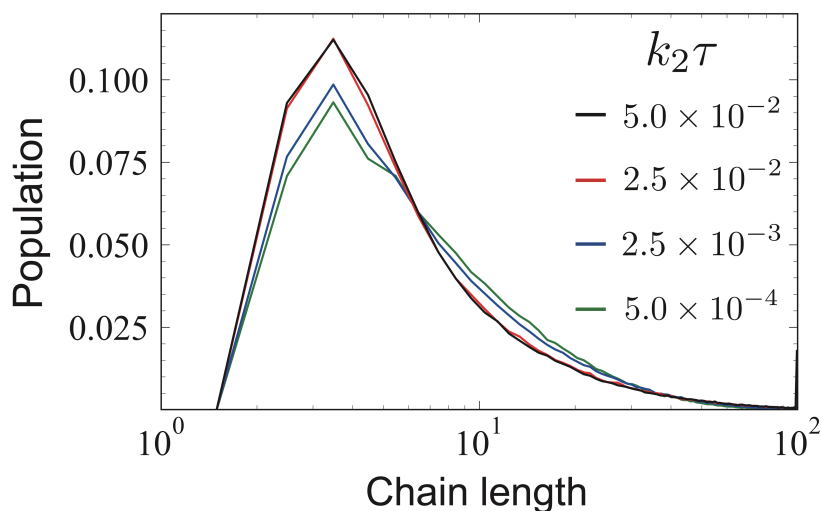


Figure 9 Distribution function of chain length distribution at conversion $\alpha = 0.1$ under different k_2 conditions.

Here, we summarize the influence of O_2 concentration on the behavior of oxidative aging. While this study varied the O_2 addition reaction rate k_2 in simulations to investigate the effect of O_2 concentration, similar control over O_2 addition reaction rate was achieved in experimental studies by adjusting O_2 partial pressure in autoclave environments [1–4]. Assuming that the onset of $[O_2]_{OER}$ corresponds to an O_2 partial pressure of 2 MPa [2], upper limit of $k_2\tau = 5.0 \times 10^{-2}$ corresponds to OER conditions, and the lower limit of $k_2\tau = 5.0 \times 10^{-4}$ corresponds to oxidative aging conditions in ambient air. In this study, the O_2 addition reaction converting $P\cdot$ to $POO\cdot$ slows down at low k_2 cases. Consequently, the effective rate of H-abstraction reactions, which are predominantly driven by $POO\cdot$ and govern the kinetics of oxidative aging, also decreases. This leads to an extended induction period and a slower reaction rate during the acceleration phase of oxidation reactions. Furthermore, the increased number of residual $P\cdot$ radicals enhances the rate of crosslinking reactions between $P\cdot$ radicals. The chain length distribution (i.e., molecular weight distribution) is also subtly affected, with

the low k_2 cases exhibiting a broader chain length range for oxidized molecular chains. This broadening can be attributed to the influence of intermolecular crosslinking reactions. These findings do not contradict behaviors investigated in the field of polymer degradation through conventional reaction kinetic approaches [1,2,21]. The spatial heterogeneity of oxidative aging diminished as k_2 decreases, provided H-abstraction reaction rate (k_3) remains constant. Since the dynamics of macroradicals ($P\cdot$, $PO\cdot$, $POO\cdot$) follow the dynamics of polymer segments, insights into the heterogeneity of oxidative aging can only be obtained through calculations of polymer dynamics. This highlights the unique contribution of such simulations in advancing our understanding of oxidative aging processes.

4. CONCLUSION

In this paper, we extended CGMD framework to perform oxidative aging simulations that reflect the effects of O_2 concentration via the reaction rate k_2 for the O_2 addition reaction. We conducted systematic simulations with varying k_2 to study O_2 concentration dependence for oxidative aging. The highest k_2 case ($k_2\tau = 5.0 \times 10^{-2}$) considered in this study corresponds to OER condition, while the lowest k_2 case ($k_2\tau = 5.0 \times 10^{-4}$) approximately corresponds to ambient air conditions. Reducing the k_2 value brings the aging system closer from the OER condition to the ambient air condition. From the aging simulations with varying k_2 , the following key findings were revealed: (i) oxidative aging reactions are retarded, (ii) heterogeneity is mitigated, and (iii) the rate of crosslinking reactions increases. Except for the reaction retardation, these results could not have been elucidated without the simulation developed in this study. Expanding this framework to address photo-aging and aging in solid-state polymer is considered important future works in the field of polymer degradation. Furthermore, integrating this simulation technique as a mesoscale simulation module into a multiscale model capable of representing the DLO effect is also a promising future direction with significant importance for real industrial applications, and we plan to publish related work in the near future.

Author Information

Corresponding Authors

Takato Ishida - Department of Materials Physics, Nagoya University, Furo-cho, Chikusa, Nagoya 464-8601, Japan; orcid. Org/0000-0003-3919-2348; E-mail: ishida@mp.pse.nagoya-u.ac.jp

Authors

Kazuya Haremakei- Department of Materials Physics, Nagoya University, Furo-cho, Chikusa, Nagoya 464-8603, Japan; orcid. Org/0009-0007-8494-8008; E-mail: haremakei.kazuya.w2@s.mail.nagoya-u.ac.jp

Yusuke Koide - Department of Materials Physics, Nagoya University, Furo-cho, Chikusa, Nagoya 464-8603, Japan; orcid. Org/0000-0002-4843-6888; E-mail: koide.yusuke.k1@f.mail.nagoya-u.ac.jp

Takashi Uneyama - Department of Materials Physics, Nagoya University, Furo-cho, Chikusa, Nagoya 464-8603, Japan; orcid. Org/0000-0001-6607-537X; E-mail: uneyama@mp.pse.nagoya-u.ac.jp

Yuichi Masubuchi - Department of Materials Physics, Nagoya University, Furo-cho, Chikusa, Nagoya 464-8603, Japan; orcid. Org/0000-0002-1306-3823; E-mail: mas@mp.pse.nagoya-u.ac.jp

Conflict of interest

The author declares no competing interests.

Acknowledgment

This work was supported by JSPS KAKENHI Grant Numbers 24K20949, 22KJ1543, "Nagoya University High Performance Computing Research Project for Joint Computational Science" in Japan, CCI holdings Co., Ltd., Mayekawa Houonkai Foundation, Suzuki Foundation, Yazaki Memorial Foundation for Science and Technology, Fujimori Science and Technology Foundation, Fuji Seal

References

1. Celina MC, Linde E, Barrett M, Ko L. Accelerated oxidation of epoxy thermosets with increased O₂ pressure. *Polymer Degradation and Stability*. 2024 Oct;228:110886.
2. Richaud E, Farcas F, Bartolomé P, Fayolle B, Audouin L, Verdu J. Effect of oxygen pressure on the oxidation kinetics of unstabilised polypropylene. *Polymer Degradation and Stability*. 2006 Feb;91(2):398–405.
3. Verdu J, Colin X, Audouin L, Rychly J, Matisová-Rychlá L. Chemiluminescence from the thermal oxidation of polyisoprene and polybutadiene I. Influence of oxygen pressure on the chemiluminescence of polyisoprene during its oxidation. *Polymer Degradation and Stability*. 2006 Jun;91(6):1387–94.
4. Coquillat M, Verdu J, Colin X, Audouin L, Nevière R. Thermal oxidation of polybutadiene. Part 1: Effect of temperature, oxygen pressure and sample thickness on the thermal oxidation of hydroxyl-terminated polybutadiene. *Polymer Degradation and Stability*. 2007 Jul;92(7):1326–33.
5. Audouin L, Gueguen V, Tcharkhtchi A, Verdu J. “Close loop” mechanistic schemes for hydrocarbon polymer oxidation. *J Polym Sci A Polym Chem*. 1995 Apr 30;33(6):921–7.
6. Richaud E, Farcas F, Fayolle B, Audouin L, Verdu J. Hydroperoxide build-up in the thermal oxidation of polypropylene – A kinetic study. *Polymer Degradation and Stability*. 2007 Jan;92(1):118–24.
7. Ishida T, Richaud E, Gervais M, Gaudy A, Kitagaki R, Hagihara H, Elakneswaran Y. Thermal aging of acrylic-urethane network: Kinetic modeling and end-of-life criteria combined with mechanical properties. *Progress in Organic Coatings*. 2022 Feb 1;163:106654.
8. Ishida T, Richaud E, Hagihara H, Kitagaki R. Estimating Network Lifetime of AUN in Photo-Aging by Kinetic Modeling and “Degelation” Model. *Macromolecular Symposia*. 2024 Aug;413(4):2300247.
9. François-Heude A, Richaud E, Desnoux E, Colin X. A general kinetic model for the photothermal oxidation of polypropylene. *Journal of Photochemistry and Photobiology A: Chemistry*. 2015 Jan;296:48–65.
10. Ernault E, Dirrenberger J, Richaud E, Fayolle B. Prediction of stress induced by heterogeneous oxidation: Case of epoxy/amine networks. *Polymer Degradation and Stability*. 2019 Apr;162:112–21.
11. Verdu J. Aspects Common to all Oxidation Processes. In: *Oxidative Ageing of Polymers* [Internet]. 2012 [cited 2024 Mar 28]. p. 17–43. Available from: <https://doi.org/10.1002/9781118562598.ch2>
12. Gee B. KINETIC STUDIES IN THE CHEMISTRY OF RUBBER AND RELATED

- MATERIALS. 111. THERMOCHEMISTRY AND MECHANISMS OF OLEFIN OXIDATION. *Trans Faraday Soc.* 1946;42:244–52.
13. Quintana A, Celina MC. Overview of DLO modeling and approaches to predict heterogeneous oxidative polymer degradation. *Polymer Degradation and Stability.* 2018 Mar;149:173–91.
 14. Ishida T, Doi Y, Uneyama T, Masubuchi Y. Modeling for Heterogeneous Oxidative Aging of Polymers Using Coarse-Grained Molecular Dynamics. *Macromolecules.* 2023 Nov 14;56(21):8474–83.
 15. Ishida T, Doi Y, Uneyama T, Masubuchi Y. Coarse-grained molecular dynamics simulation of oxidative aging of polymers -effect of free radical diffusivity -. *Polym J* [Internet]. 2024 Aug 1 [cited 2024 Aug 19]; Available from: <https://www.nature.com/articles/s41428-024-00942-5>
 16. Kremer K, Grest GS. Dynamics of entangled linear polymer melts: A molecular-dynamics simulation. *The Journal of Chemical Physics.* 1990 Apr 15;92(8):5057–86.
 17. Richaud Emmanuel. *Durabilité des Géotextiles en Polypropylène* [Engineering Sciences]. [Paris]: Arts et Métiers ParisTech; 2006.
 18. Plimpton S. Fast Parallel Algorithms for Short-Range Molecular Dynamics. *Journal of Computational Physics.* 1995;117(1):1–19.
 19. Gissinger JR, Jensen BD, Wise KE. REACTER: A Heuristic Method for Reactive Molecular Dynamics. *Macromolecules.* 2020 Nov 24;53(22):9953–61.
 20. Gissinger JR, Nikiforov I, Afshar Y, Waters B, Choi M ki, Karls DS, Stukowski A, Im W, Heinz H, Kohlmeyer A, Tadmor EB. Type Label Framework for Bonded Force Fields in LAMMPS. *J Phys Chem B.* 2024 Mar 20;acs.jpcc.3c08419.
 21. François-Heude A, Richaud E, Guinault A, Desnoux E, Colin X. Impact of oxygen transport properties on polypropylene thermal oxidation, part 1: Effect of oxygen solubility. *J of Applied Polymer Sci.* 2015 Feb 5;132(5):app.41441.
 22. Okamba-Diogo O, Richaud E, Verdu J, Fernagut F, Guilment J, Fayolle B. Molecular and macromolecular structure changes in polyamide 11 during thermal oxidation – Kinetic modeling. *Polymer Degradation and Stability.* 2015 Oct;120:76–87.
 23. Linde E, Nilsson F, Barrett M, Hedenqvist MS, Celina MC. Time- and Feedback-Dependent DLO Phenomena in Oxidative Polymer Aging. *Polymer Degradation and Stability.* 2021 Jul;189:109598.
 24. White JR, Shyichuk AV. Macromolecular scission and crosslinking rate changes during polyolefin photo-oxidation. *Polymer Degradation and Stability.* 2007 Jul;92(7):1161–8.
 25. He X, Zhang Z, Ren T, Yue X, Wang S. Oxygen diffusion effects in thermo-oxidative degradation of typical tire rubber. *Polymer Degradation and Stability.* 2024 Dec;230:111074.
 26. Taourit S, Gac PYL, Bourdet A, Van Elslander A, Robin C, Fayolle B. Changes in natural rubber mechanical behavior during oxidation: Relationship with oxygen consumption. *Polymer Degradation and Stability.* 2024 Jul;225:110787.
 27. Celina MC, Linde E, Martinez E. Carbonyl Identification and Quantification Uncertainties

for Oxidative Polymer Degradation. *Polymer Degradation and Stability*. 2021 Jun;188:109550.
28. Gartner TE, Jayaraman A. Modeling and Simulations of Polymers: A Roadmap. *Macromolecules*. 2019 Feb 12;52(3):755–86.

Supporting information

Coarse-Grained Molecular Dynamics Simulations for Oxidative Aging of Polymers under Various O₂ Concentrations

*Takato Ishida**, *Kazuya Haremake*, *Yusuke Koide*, *Takashi Uneyama*, *Yuichi Masubuchi*

Department of Materials Physics, Nagoya University, Furo-cho, Chikusa, Nagoya 464-8603, Japan

Tel: +81-52-789-4202, Mobile:+81-90-1145-4372

E-mail address: ishida@mp.pse.nagoya-u.ac.jp

TABLE OF CONTENTS

1. **Normalized time evolution of chemical kinetic behaviors** ----- S3, S4

1. Normalized time evolution of chemical kinetic behaviors

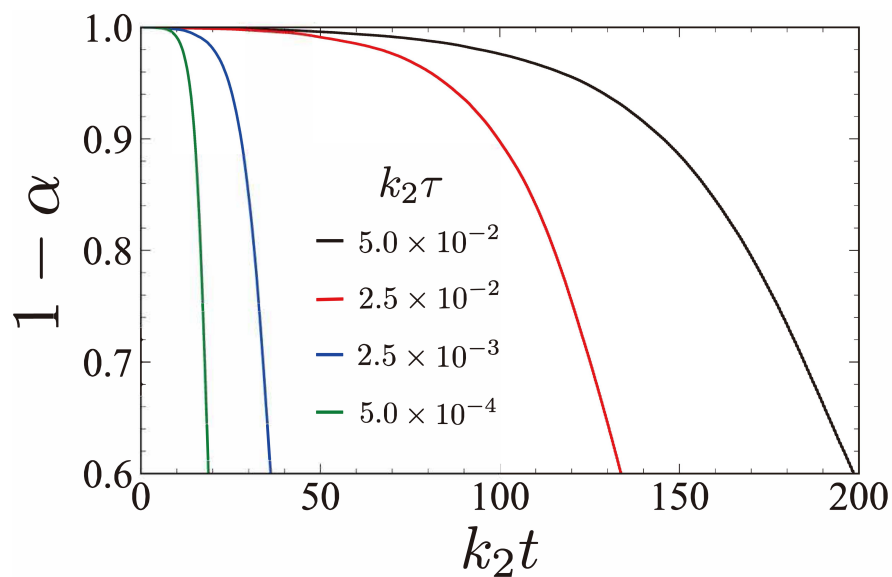


Figure S1 Relationship between conversion (α) and the time normalized by the O_2 addition reaction rate ($k_2 t$) at various k_2 cases.

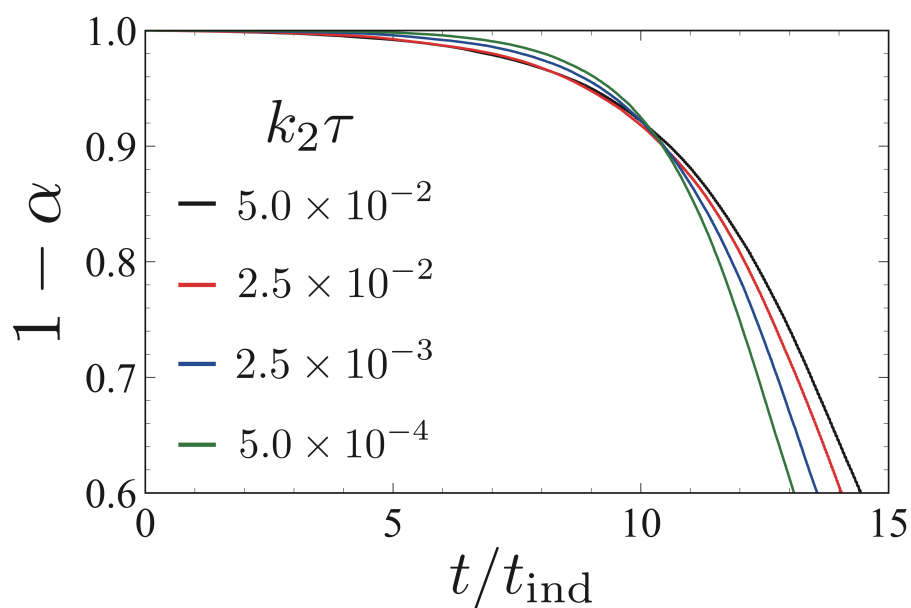


Figure S2 Relationship between conversion (α) and dimensionless time (t/t_{ind}) at various k_2 cases.

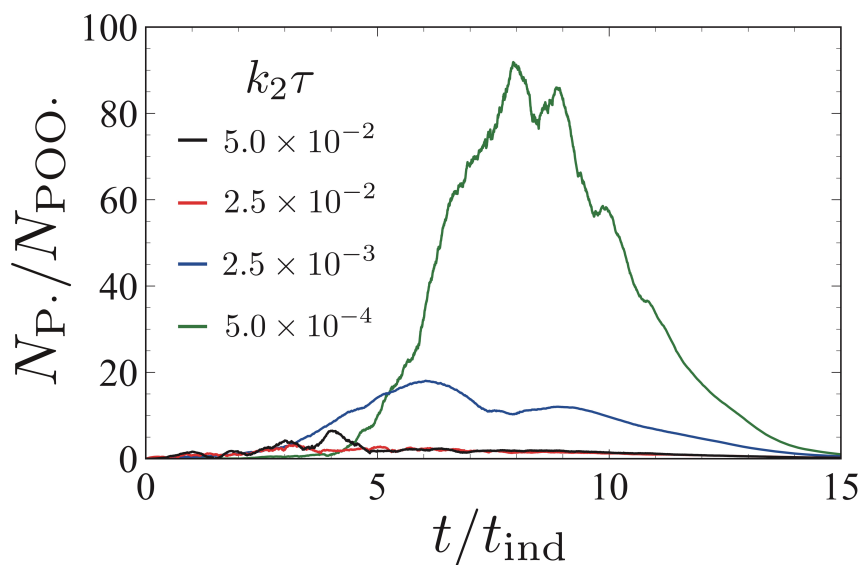


Figure S3 Time evolution of the ratio of P· to POO· radicals ($N_{P\cdot}/N_{POO\cdot}$) as a function of t/t_{ind} at various k_2 cases.

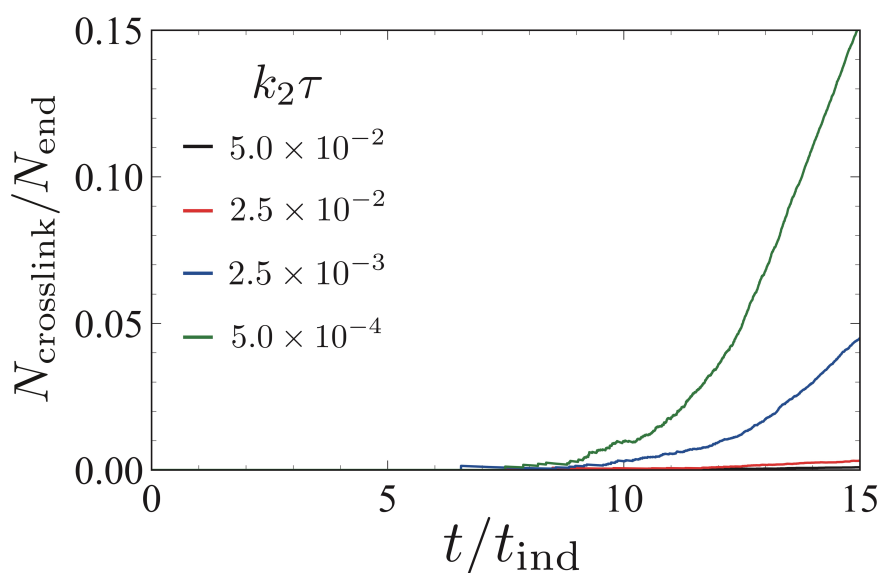


Figure S4 Time evolution of the ratio of crosslink to scission end counts ($N_{crosslink}/N_{end}$) as a function of t/t_{ind} at various k_2 cases.